Numerical Calculation of the Dynamic Dipole Coefficient and Electrorotation Velocity of Cells

Viviana Zimmerman,*,† Constantino Grosse,†,‡ and Vladimir N. Shilov§

Departamento de Física, Universidad Nacional de Tucumán, Av. Independencia 1800, (4000) S.M. de Tucumán, Argentina, Consejo Nacional de Investigaciones Cientıficas y Técnicas, Argentina, and Institute of Biocolloid Chemistry, Ukrainian Academy of Sciences, Kiev, Ukraine

Received: June 6, 2003; In Final Form: August 15, 2003

The electric potential, ion number concentration, and fluid velocity distributions induced by an ac electric field applied to a cell suspended in an electrolyte solution are numerically calculated, using a network simulation method. The cell model consists of a conducting internal medium surrounded by an insulating membrane and a charged permeable cell wall. The distributions obtained are used to calculate the dipole coefficient and the electrorotation velocity of the particles under the action of a rotating field. The results are first particularized to simple systems, leading to good agreement with existing theories. Then, the dependence of the rotation spectra of cells with some of the parameters is considered.

1. Introduction

Although numerical methods have been widely used to study the dielectric and electrokinetic properties of colloidal particle suspensions, most of those studies deal with homogeneous particles,[1−5] or the so-called soft particles,[6,7] used in general to model uncoated and coated latex-type particles, respectively. On the other hand, the properties, behavior, and management of suspended biological particles under the action of electric fields have also been widely studied due to the need to understand, analyze, and manipulate this type of particles. However, these studies are mainly experimental[8−13] or theoretical[14−16] but, to our knowledge, not numerical.

In the present paper a numerical method is used to solve the electric potential, ion number concentration, and fluid velocity distributions induced by an ac electric field applied to a cell suspended in an electrolyte solution. The cell model consists of a conducting internal medium surrounded by an insulating membrane and a charged permeable cell wall. Using the distributions obtained, electrorotation spectra are predicted for these particles. The same distributions can also be used to predict other electrokinetic phenomena or the dielectric behavior of suspensions, which will be considered in a following paper.

The numerical method used is based on a network simulation method which has been successfully applied over the past few years to study different aspects of the dielectric and electrokinetic properties of electrolyte solutions and colloidal systems,[5,17−19] and was recently applied to the prediction of electrorotation spectra of latex-type particles.[20] The procedure consists of discretizing the domain and the differential equations, as in the lineal finite difference method, and establishing the similitude between the discretizated equations in every differential region and the equations that represent an elementary electric circuit composed of basic electronic components (resistors, capacitors, and current and voltage sources). Hence, the solution of the original problem is reduced to the solution of potentials and currents in a network composed of a set of these elementary subcircuits. The direct solution of the governing differential equations is thus avoided, and any commercially available circuit analysis software can be employed to obtain the dynamic behavior of the system.

2. Electric Potential and Ion Concentrations

The system considered in the present work corresponds, as previously said, to a cell suspended in an electrolyte solution. The cell is modeled as a spherical conductive particle surrounded by a nonconductive shell representing the membrane and by an external uniformly charged conductive shell representing the cell wall (Figure 1). The following hypotheses are, moreover, assumed on the system:

(•) The conductivity of the membrane is considered null, so the interfaces at $r = R_b$ and $r = R_c$ are impermeable to the ions.

(•) Only two types of ions are considered for every conductive medium.

(•) The cell wall is generally composed of a porous material that allows the exchange of ions with the external medium and has been previously modeled as an ion-exchange resin.[21]

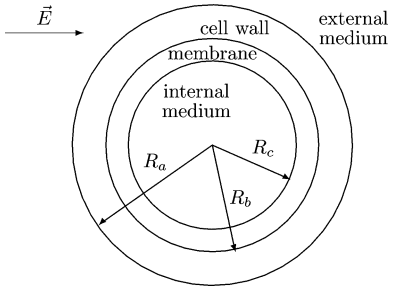

Figure 1. Model considered for the cell. The internal layer (membrane) is nonconductive, whereas all the other media are conductive. The external layer (cell wall) has a uniformly distributed density of fixed charge and is in equilibrium with the external medium. So, the interfaces at $r = R_b$ and $r = R_c$ are impermeable to the ions, whereas the interface at $r = R_a$ is totally permeable to the ions.

* Corresponding author. E-mail: vzimmerman@herrera.unt.edu.ar.
† Universidad Nacional de Tucumán.
‡ Consejo Nacional de Investigaciones Cientıficas y Técnicas.
§ Ukrainian Academy of Sciences.

10.1021/jp035612v CCC: $25.00
Published on Web 11/25/2003

Consequently, the external shell is considered conductive, with a uniform distribution of fixed charges and with the interface at $r = R_a$ perfectly permeable to the ions.

(•) As a consequence of the preceding hypothesis, the wall and the external medium are in equilibrium, so the valences of the mobile ions are the same in both media.

(•) The wall and external medium permittivities are assumed to be identical in order to avoid the calculation of the Born energy term in the Poisson equation.[22]

(•) The hydrodynamic permeability of the wall is sufficiently low to impede liquid flow in this region. However, the ions can move inside the wall (with a mobility possibly different from the mobility in the external medium), since it is assumed to be conductive.

(•) Due to a possible structure present in the internal part of the cell, the viscosity in the internal medium is considered high enough to impede the liquid flow.

According to these hypotheses, the electric potential and ion number concentrations are obtained by solving the following equation system:

• Laplace equation:

$$\nabla^2\phi(\vec{r},t) = 0, \quad R_c < r < R_b \tag{1}$$

• Poisson equation:

$$\nabla^2\phi(\vec{r},t) = -\frac{e}{\epsilon_o \epsilon_j}\left(z_j^+ C^+(\vec{r},t) + z_j^- C^-(\vec{r},t)\right) - \overbrace{\frac{e}{\epsilon_o \epsilon_e} z^f C^f}^{R_b<r<R_a}, \quad 0 < r < R_c,\ R_b < r < \infty,\ j = \mathrm{e,i} \tag{2}$$

• Nernst−Planck equations:

$$\vec{j}^{\pm}(\vec{r},t) = -D_j^{\pm}\nabla C^{\pm}(\vec{r},t) - \frac{ez_j^{\pm}D_j^{\pm}}{kT} C^{\pm}(\vec{r},t)\,\nabla\phi(\vec{r},t) + \overbrace{C^{\pm}(\vec{r},t)\,\vec{v}(\vec{r},t)}^{R_a<r<\infty}, \quad 0 < r < R_c,\ R_b < r < \infty,\ j = \mathrm{e,w,i} \tag{3}$$

• Continuity equations:

$$\nabla\cdot\vec{j}^{\pm}(\vec{r},t) = -\frac{\partial C^{\pm}(\vec{r},t)}{\partial t}, \quad 0 < r < R_c, \quad R_b < r < \infty \tag{4}$$

• Navier−Stokes equation:

$$\eta\nabla^2\vec{v}(\vec{r},t) - \nabla p(\vec{r},t) = e(z_e^+ C^+(\vec{r},t) + z_e^- C^-(\vec{r},t))\nabla\phi(\vec{r},t) + \rho^m\left[\frac{\partial\vec{v}(\vec{r},t)}{\partial t} + (\vec{v}(\vec{r},t)\cdot\nabla)\vec{v}(\vec{r},t)\right], \quad R_a < r < \infty \tag{5}$$

• Incompressibility equation:

$$\nabla\cdot\vec{v}(\vec{r},t) = 0, \quad R_a < r < \infty \tag{6}$$

where $\phi(\vec{r},t)$ is the electric potential, $C^{\pm}(\vec{r},t)$ are the number concentrations of positive and negative ions, $\vec{v}(\vec{r},t)$ is the velocity of the electrolyte solution, $p(\vec{r},t)$ is the pressure, $z_j^{\pm}$, $D_j^{\pm}$, and $\vec{j}^{\pm}(\vec{r},t)$ are the signed valences, diffusion coefficients, and fluxes of positive and negative ions, C^f and z^f are the number concentration and signed valence of fixed charges in the wall, η and ρ^m are the viscosity and mass density of the electrolyte solution, ϵ_j and ϵ_0 are the relative permittivity and the permittivity of free space, e is the elementary charge, k is the Boltzmann constant, T is the temperature, and the subindexes e, w, and i stand for the external medium, wall, and internal medium, respectively.

The solution of the equation system is simplified by separating it into equilibrium and nonequilibrium parts. These parts have different symmetries and can be obtained by expressing the electric potential and ion number concentrations as follows:

$$\phi(\vec{r},t) = \phi_0(r) + \delta\phi(\vec{r},t) \tag{7}$$

$$C^{\pm}(\vec{r},t) = C_0^{\pm}(r) + \delta C^{\pm}(\vec{r},t) \tag{8}$$

where $C_0^{\pm}(r)$ and $\phi_0(r)$ are the equilibrium ion number concentrations and electric potential distributions, which only depend on the distance to the particle due to the spherical symmetry of the equilibrium problem, while $\delta C^{\pm}(\vec{r},t)$ and $\delta\phi(\vec{r},t)$ are the changes induced by the field on the same distributions. Moreover, some numerical problems are overcome using a new set of variables defined in terms of a virtual system (usually called *thermostat*) which is everywhere neutral and in local equilibrium with the real system.[20,23,24] The new variables are

$$\frac{\delta c(\vec{r},t)}{c_\infty} + z^{\pm}\tilde{\varphi}(\vec{r},t) = \frac{\delta C^{\pm}(\vec{r},t)}{C_0^{\pm}(r)} + z^{\pm}\delta\tilde{\phi}(\vec{r},t) \tag{9}$$

$$\delta\tilde{\phi}(\vec{r},t) = \tilde{\varphi}(\vec{r},t) + \tilde{\Phi}(\vec{r},t) \tag{10}$$

where the mark ∼ placed over the potentials stands for their dimensionless forms:

$$\tilde{\phi}(\vec{r},t) = \frac{e}{kT}\phi(\vec{r},t)$$

c_∞ and $\delta c(\vec{r},t)$ are the equilibrium and the field induced change of the electrolyte concentration in the thermostat. $\tilde{\varphi}(\vec{r},t)$ is the dimensionless electric potential in the thermostat, and $\tilde{\Phi}(\vec{r},t)$ is the so-called *quasiequilibrium* dimensionless potential. The quasiequilibrium potential is a short-range function, so it has zero value far from the particle, making the real system and the thermostat identical in that region.

Substituting eqs 7−10 into the equation system, and keeping only linear terms in the field due to the hypothesis of weak fields, the system reduces to

Equilibrium equations:

$$\frac{1}{r^2}\frac{d}{dr}\left(r^2\frac{d\tilde{\phi}_0(r)}{dr}\right) = \frac{-e^2}{\epsilon_o\epsilon_j kT}\left(z_j^+ C_0^+(r) + z_j^- C_0^-(r)\right) - \overbrace{\frac{e^2}{\epsilon_o\epsilon_j kT} z^f C^f}^{R_b<r<R_a}, \quad 0 < r < R_c,\ R_b < r < \infty,\ j = \mathrm{e,i} \tag{11}$$

$$\frac{1}{r^2}\frac{\mathrm{d}}{\mathrm{d}r}\left(r^2\frac{\mathrm{d}\tilde{\phi}_0(r)}{\mathrm{d}r}\right) = 0, \quad R_c < r < R_b \tag{12}$$

where

$$C_0^{\pm}(r) = \begin{cases} c_{e\infty}^{\pm}\exp(-z_e^{\pm}\tilde{\phi}_0(r)), & R_b < r < \infty \\ c_{io}^{\pm}\exp(-z_i^{\pm}(\tilde{\phi}_0(r) - \tilde{\phi}_{eq})), & 0 < r < R_c \end{cases}$$

$c_{e\infty}^{\pm}$ are the equilibrium number concentrations of positive and negative ions in the electroneutral electrolyte solution outside the double layer, while $c_{io}^{\pm}$ are the equilibrium number concen-

trations of positive and negative ions in an electroneutral solution that is in thermodynamic equilibrium with the internal medium. The electric potential of this electroneutral solution has in general a nonzero value denoted as $\tilde{\phi}_{eq}$.

Nonequilibrium equations:

$$\frac{1}{r^2}\frac{\partial}{\partial r}\left(r^2\frac{\partial\tilde{\varphi}}{\partial r}\right)-\frac{2}{r^2}\tilde{\varphi}=-\frac{\Lambda_j}{D_j^{ef}}\frac{\partial}{\partial t}\left(\frac{\delta c}{c_\infty}\right)-\frac{Q_j}{D_j^{ef}}\frac{\partial\tilde{\Phi}}{\partial t}+\frac{d\tilde{\phi}_0}{dr}\left[\frac{\partial}{\partial r}\left(\frac{\delta c}{c_\infty}\right)+(z_j^+ + z_j^-)\frac{\partial\tilde{\varphi}}{\partial r}\right]-\overbrace{\frac{Q_e}{D_e^{ef}}\frac{d\tilde{\phi}_0}{dr}v_r}^{R_a<r<\infty},$$

$$0<r<R_c,\ R_b<r<\infty,\ j=e,w,i \quad (13)$$

$$\frac{1}{r^2}\frac{\partial}{\partial r}\left(r^2\frac{\partial\delta\tilde{\phi}}{\partial r}\right)-\frac{2}{r^2}\delta\tilde{\phi}=0,\quad R_c<r<R_b \quad (14)$$

$$\frac{1}{r^2}\frac{\partial}{\partial r}\left[r^2\frac{\partial}{\partial r}\left(\frac{\delta c}{c_\infty}\right)\right]-\frac{2}{r^2}\frac{\delta c}{c_\infty}=\frac{1}{D_j^{ef}}\frac{\partial}{\partial t}\left(\frac{\delta c}{c_\infty}\right)-z_j^+z_j^-\frac{\Lambda_j}{D_j^{ef}}\frac{\partial\tilde{\Phi}}{\partial t}-z_j^+z_j^-\frac{d\tilde{\phi}_0}{dr}\frac{\partial\tilde{\varphi}}{\partial r}-\overbrace{z_e^+z_e^-\frac{\Lambda_e}{D_e^{ef}}\frac{d\tilde{\phi}_0}{dr}v_r}^{R_a<r<\infty},\ 0<r<R_c,\ R_b<r<\infty,\ j=e,w,i \quad (15)$$

$$\frac{1}{r^2}\frac{\partial}{\partial r}\left(r^2\frac{\partial\tilde{\Phi}}{\partial r}\right)-\frac{2}{r^2}\tilde{\Phi}=\frac{\Lambda_j}{D_j^{ef}}\frac{\partial}{\partial t}\left(\frac{\delta c}{c_\infty}\right)+\frac{Q_j}{D_j^{ef}}\frac{\partial\tilde{\Phi}}{\partial t}-\frac{d\tilde{\phi}_0}{dr}\left[\frac{\partial}{\partial r}\left(\frac{\delta c}{c_\infty}\right)+(z_j^+ + z_j^-)\frac{\partial\tilde{\varphi}}{\partial r}\right]+\overbrace{\frac{Q_e}{D_e^{ef}}\frac{d\tilde{\phi}_{e0}}{dr}v_r}^{R_a<r<\infty}-\frac{e^2}{\epsilon_o\epsilon_j kT}\left[\left(z_j^+C_0^+ + z_j^-C_0^-\right)\frac{\delta c}{c_\infty}-\left[(z_j^+)^2C_0^+ + (z_j^-)^2C_0^-\right]\tilde{\varphi}\right],$$

$$0<r<R_c,\ R_b<r<\infty,\ j=e,w,i \quad (16)$$

$$\frac{\eta}{r^2}\frac{\partial}{\partial r}\left(r^2\frac{\partial b}{\partial r}\right)-\frac{2\eta}{r^2}b=\rho^m\frac{\partial b}{\partial t}+\frac{kT}{r}\frac{d\tilde{\phi}_0}{dr}\left[(z_e^+C_0^+ + z_e^-C_0^-)\frac{\delta c}{c_\infty}+[(z_e^+)^2C_0^+ + (z_e^-)^2C_0^-]\tilde{\varphi}\right]$$

$$R_a<r<\infty \quad (17)$$

$$b=-\frac{r}{2}\frac{\partial^2 v_r}{\partial r^2}-2\frac{\partial v_r}{\partial r},\quad R_a<r<\infty \quad (18)$$

where

$$\Lambda_j=\frac{D_j^+-D_j^-}{D_j^+z_j^+-D_j^-z_j^-} \quad (19)$$

$$D_j^{ef}=\frac{D_j^+D_j^-(z_j^+-z_j^-)}{D_j^+z_j^+-D_j^-z_j^-}\quad j=e,w,i \quad (20)$$

$$Q_j=\frac{z_j^+D_j^--z_j^-D_j^+}{D_j^+z_j^+-D_j^-z_j^-} \quad (21)$$

$D_j^{\pm}$ are the diffusion coefficients in each medium, and $\vec{b}(\vec{r},t)=$ curl $\vec{v}(\vec{r},t)$ is the vorticity, introduced to avoid the calculation of the pressure.

The explicit angular dependences of the variables used to write eqs 11−18,

$$\tilde{\varphi}(\vec{r},t)=\tilde{\varphi}(r,t)\cos\theta$$
$$\tilde{\Phi}(\vec{r},t)=\tilde{\Phi}(r,t)\cos\theta$$
$$\delta c(\vec{r},t)=\delta c(r,t)\cos\theta$$
$$\vec{v}(\vec{r},t)=v_r(r,t)\cos\theta\,\hat{e}_r-v_\theta(r,t)\sin\theta\,\hat{e}_\theta$$
$$\vec{b}(\vec{r},t)=b(r,t)\sin\theta\,\hat{e}_\varphi$$

result in view of the axial symmetry of the problem and considering that the applied field is uniform,

$$\vec{E}(\vec{r},t)=E(t)(\cos\theta\hat{e}_r-\sin\theta\hat{e}_\theta) \quad (22)$$

and, furthermore, that it is weak. These hypotheses, implicitly used in most electrorotation theories, are valid if the applied field is uniform within the region where all the field induced changes occur (This is a region of radius $\sim 2(R_a+1/\kappa_e)$,[25] where κ_e is the reciprocal of the Debye screening length in the external medium: $\kappa_e=[e^2[(z_e^+)^2c_{e\infty}^+ + (z_e^-)^2c_{e\infty}^-]/(\epsilon_0\epsilon_e kT)]^{1/2}$.) and if the field induced change of the electrolyte concentration is everywhere small: $\delta c \ll c_\infty$. This last condition is satisfied if $EeR_a/kT \ll 1$, or $E \ll 10000$ V/m for micron sized particles.[24]

The explicit dependence with r and t in the nonequilibrium equation system was omitted to simplify the notation, while the angular variable θ cancels out in every one of those equations, so the solutions are valid for any value of θ. Moreover, it can be noted that the equation system does not depend explicitly on the tangential component of the velocity ($v_\theta(r,t)$), since it was replaced in terms of the radial component ($v_r(r,t)$) using the incompressibility equation (eq 6).

2.1. Boundary Conditions. The boundary conditions used for the solution of the equation system are as follows:

(•) Equilibrium potential ($\tilde{\phi}_0(r)$). It vanishes at infinity and is continuous over the whole space. Due to the central symmetry of the system in equilibrium, its derivative is null at $r=0$. Moreover, the normal component of the equilibrium displacement is also continuous over the whole space because there are no fixed surface charges.

(•) Field induced change of the electric potential ($\delta\tilde{\phi}(r,t)$). Its value at infinity is defined by the applied field ($-eE(t)\,r/kT$), whereas it is null for $r=0$ due to symmetry. The electric potential and the normal component of the displacement are continuous over the whole space.

(•) Field induced change of the ion number concentrations ($\delta C^{\pm}(r,t)$). They vanish at infinity, since there is no applied concentration gradient, and also at $r=0$ due to symmetry. The conditions at the interfaces between the different media are defined in terms of the fluxes of ions ($\vec{J}^{\pm}(r,t)$) and dimensionless electrochemical potentials,

$$\delta\tilde{\mu}^{\pm}(\vec{r},t)=\frac{\delta C^{\pm}(\vec{r},t)}{C_0^{\pm}(r)}+z_j^{\pm}\,\delta\tilde{\phi}(\vec{r},t) \quad (23)$$

At the wall outer interface, the normal component of the fluxes, and the dimensionless electrochemical potentials are continuous, while at the membrane interfaces the normal components of the fluxes are null because the interfaces are impermeable to the ions.

(•) Radial component of the velocity ($v_r(r,t)$). At infinity it tends to a constant value v_∞. The nonslipping condition on the surface of the impermeable particle together with the incom-

pressibility of the fluid lead to

$$\left.\frac{\partial v_r(r,t)}{\partial r}\right|_{r=R_a+} = 0$$

where the symbol + after R_a stands for the derivative from the right of the interface.

(•) Vorticity ($b(r,t)$). At infinity it is null, and the balance of forces on the particle surface leads to

$$b(R_a+,t) - R_a \left.\frac{\partial b(r,t)}{\partial r}\right|_{R_a+} = \frac{R_a \Delta\rho}{\eta}\frac{\partial v_r(R_a+,t)}{\partial t} + \frac{kT}{R_a^2\eta}\int_{R_a}^{\infty}[z_e^+ C_0^+(r)\,\delta\tilde{\mu}^+(r,t) + z_e^- C_0^-(r)\,\delta\tilde{\mu}^-(r,t)]\frac{d\tilde{\phi}_0(r)}{dr} r^2\,dr \quad (24)$$

where $\Delta\rho$ is the difference between the mass density of the external medium and the average mass density of the particle. This equation has been obtained taking into account inertial terms that are important for high-frequency fields, according to the description presented in ref 3 (see the Appendix), and corrects the boundary condition presented in ref 5 which contains minus the particle mass density instead of the difference $\Delta\rho$.

2.2. Electric Potential in the Membrane. In the nonconducting shell that represents the membrane, the electric potential is described just by the Laplace equation (eqs 12 and 14). As a consequence, an exact analytic solution exists for this region and can be used instead of the numerical method. Thus, the equilibrium potential and field induced variation of the potential in the membrane are

$$\tilde{\phi}_0(r) = -\frac{A_0}{r} + B_0 \quad R_c < r < R_b \quad (25)$$

$$\delta\tilde{\phi}(r,t) = \frac{AE(t)}{r^2} - BE(t)r \quad R_c < r < R_b \quad (26)$$

where A_0, B_0, A, and B are integration constants, usually obtained using boundary conditions. However, since the electric potential in all the other regions that form the system is obtained using a numerical method, these constants cannot be directly calculated, but they are rather eliminated replacing the membrane potential expressions in the boundary conditions. Hence, the first of these equations (eq 25) is substituted into the conditions of continuity of the equilibrium potential and continuity of the normal component of the equilibrium displacement, at $r = R_b$ and $r = R_c$. A system composed by four equations is obtained and, eliminating A_0 and B_0 among them, the following new boundary conditions result for the equilibrium potential:

$$\tilde{\phi}_0(R_c-) = \tilde{\phi}_0(R_b+) - \frac{R_c(R_b - R_c)}{R_b}\frac{\epsilon_i}{\epsilon_m}\left.\frac{d\tilde{\phi}_0(r)}{dr}\right|_{R_c-} \quad (27)$$

$$\left.\frac{d\tilde{\phi}_0(r)}{dr}\right|_{R_b+} = \frac{R_c^2}{R_b^2}\frac{\epsilon_i}{\epsilon_e}\left.\frac{d\tilde{\phi}_0(r)}{dr}\right|_{R_c-} \quad (28)$$

Following a similar procedure with eq 26 (substituting in the conditions of continuity of the field induced change of the electric potential and continuity of the normal component of the displacement, at $r = R_b$ and $r = R_c$), the following new boundary conditions are obtained for the field induced change of the electric potential:

$$\delta\tilde{\phi}(R_c-,t) = \frac{3R_b^2R_c}{2R_b^3 + R_c^3}\delta\tilde{\phi}(R_b+,t) - \frac{R_c(R_b^3 - R_c^3)}{(2R_b^3 + R_c^3)}\frac{\epsilon_i}{\epsilon_m}\left.\frac{\partial\delta\tilde{\phi}(r,t)}{\partial r}\right|_{R_c-} \quad (29)$$

$$\left.\frac{\partial\delta\tilde{\phi}(r,t)}{\partial r}\right|_{R_b+} = \frac{2(R_b^3 - R_c^3)}{R_b(2R_b^3 + R_c^3)}\frac{\epsilon_m}{\epsilon_e}\delta\tilde{\phi}(R_b+,t) + \frac{3R_c^3\epsilon_i}{(2R_b^3 + R_c^3)\epsilon_e}\left.\frac{\partial\delta\tilde{\phi}(r,t)}{\partial r}\right|_{R_c-} \quad (30)$$

where ϵ_m is the membrane relative permittivity and, again, the symbols ± after R_b and R_c stand for derivatives from the right and left of the interfaces, respectively.

2.3. Numerical Calculations. The numerical calculations were performed in a similar way as in previous works.[5,19,20] The spatial variable r was replaced by new dimensionless variables ξ that tend to linearize the dependence of the unknown magnitudes, and the domain was then discretized into a finite number of compartments.

The choice of the variables ξ depends on the behavior of the unknown magnitudes, so different variables were used for each medium and also for the solution of the equilibrium and nonequilibrium problems. For the equilibrium problem, spatial variables ξ with an exponential close range behavior were used:

$$\xi_e = \frac{R_a}{r}[1 + \kappa_e R_a \exp[\kappa_e(R_a - r)]]$$

$$\xi_w = C_{1w}r + C_{2w}\exp[\kappa_w(R_b - r)] + C_{3w}$$

$$\xi_i = C_{1i}r + C_{2i}\exp(\kappa_i(r - R_c)) + C_{3i}$$

where

$$\kappa_w = [e^2[(z_e^+)^2 c_{e\infty}^+ + (z_e^-)^2 c_{e\infty}^- + (z_f)^2 C^f]/(\epsilon_0\epsilon_e kT)]^{1/2}$$

$$\kappa_i = [e^2[(z_i^+)^2 c_{io}^+ + (z_i^-)^2 c_{io}^-]/(\epsilon_0\epsilon_i kT)]^{1/2}$$

and the coefficients C_{jw} and C_{ji} are included in the Supporting Information. For nonequilibrium, not only the spatial variables in the external and internal media were changed,

$$\xi_e = \frac{R_a}{r}$$

$$\xi_i = 1 - \frac{r}{R_c}$$

but also the dependent variables were replaced by new dimensionless variables with a linear long distance dependence on ξ. Thus, the dimensionless dependent variables used in the external medium are

$$f(r,t) = \frac{r}{R_a}\left(\tilde{\varphi}(r,t) + \frac{eE(t)}{kT}r\right)$$

$$q(r,t) = \frac{r}{R_a}\tilde{\Phi}(r,t)$$

$$n(r,t) = \frac{r}{R_a}\frac{\delta c(r,t)}{c_\infty}$$

$$u(r,t) = \frac{r^2}{R_a D_{ef}}(v_r(r,t) - v_\infty)$$

$$B(r,t) = \frac{R_a^2}{D_{ef}}b(r,t)$$

while for the wall and internal medium

$$f(r,t) = \tilde{\varphi}(r,t) + \frac{eE(t)}{kT}r$$

$$q(r,t) = \tilde{\Phi}(r,t)$$

$$n(r,t) = \frac{\delta c(r,t)}{c_\infty}$$

Substituting all the new variables in the equation system (eqs 11−18) and boundary conditions, and after discretization, the network circuits were designed in a similar way as in refs 5 and 20 (see Supporting Information). For the circuits design, the domain corresponding to the external medium was divided into three regions determined by the ζ-potential value (equilibrium potential at $r = R_a$) and by the double-layer thickness ($1/\kappa_e$). In the cell wall the domain was also divided into three regions, but determined by the screening length $1/\kappa_w$ next to both interfaces. Finally, in the internal medium, the domain was divided into two regions only, determined by the double-layer thickness in this medium ($1/\kappa_i$). Each of these regions was then subdivided into small compartments, where the spatial variation of the functions is assumed to be linear. The width of the compartments ($\Delta\xi$) is constant over every region. The complete network was finally analyzed using a circuits analyzer software. The input file with the description of the circuit and the output file with the potential values in the circuit were created and interpreted, respectively, using C language programs that are available upon request.

3. Electrorotation Velocity

The electrorotation velocity is calculated using the equation previously obtained,[20]

$$\Omega = -\frac{\epsilon_0\epsilon_e E}{2\eta R_a^3}\lim_{r\to\infty}[r^2\,\mathrm{Im}\{\delta\phi(r) + Er\}] - \frac{1}{3\eta}\int_{R_a}^{\infty}\left(1 - \frac{x^3}{R_a^3}\right)g(x)\,\mathrm{d}x \quad (31)$$

where the limit in the first term is proportional to the imaginary part of the dipole coefficient, and

$$g(r) = \frac{e}{2r}[\mathrm{Re}\{z_j^+\delta C^+(r) + z_j^-\delta C^-(r)\}\,\mathrm{Im}\{\delta\phi(r)\} - \mathrm{Im}\{z_j^+\delta C^+(r) + z_j^-\delta C^-(r)\}\,\mathrm{Re}\{\delta\phi(r)\}] \quad (32)$$

When the diffusion related processes are neglected in the problem, eq 31 reduces to the classical expression for the electrorotation velocity of a spherical particle[26] (given by the first term of the equation). In this limit, the field induced changes of the ion concentrations are located within infinitesimally thin layers near the interfaces and, consequently, the integral in the second term of the equation is null. This second term represents the electroosmotic contribution to electrorotation, valid for any value of the double-layer thickness.[20]

The electrorotation velocity is calculated by substituting in eqs 31 and 32 the numerical results for the ion concentration and potential distributions obtained in the previous section and by evaluating numerically the integral (using a trapezoidal method).

4. Results and Discussion

In the first place, and before analyzing the numerical electrorotation spectra obtained for cells, the numerical results are particularized for some limiting cases that represent systems that, to our knowledge, were not numerically solved before with an applied ac electric field. Therefore, comparisons between some theoretical predictions and the corresponding numerical results are presented. Figure 2 shows the real part of the electrophoretic mobility spectra of a particle consisting of an insulating sphere (internal medium set identical to the membrane) surrounded by the wall. This system is suitable to represent the so-called soft particles in the limit of a very low hydrodynamic permeability in the polymer layer. Ohshima has extensively studied the electrokinetic behavior of soft particles and formulated a theory for their dynamic electrophoretic mobility.[27] Moreover, he particularized his theory for very low ζ-potentials and derived an approximate formula, that we have used setting the parameter that specifies the convection in the polymer layer to a very high value, for comparison with our numerical results. Each spectrum in the figure corresponds to different values of the fixed charge density and polymer layer thickness. As expected, numerical and theoretical spectra are in good agreement for very weakly charged particles, but important differences already appear at ζ-potential values of $\sim$10 mV.

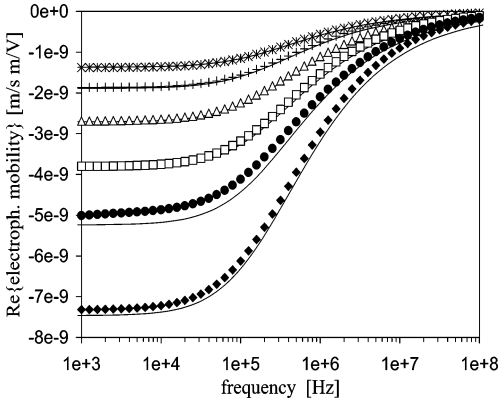

Figure 2. Real part of the electrophoretic mobility spectra of a soft particle. Comparison between numerical results (symbols) and theoretical predictions according to Ohshima[27] (full lines). The different curves correspond to different values of the fixed charge density and polymer layer thickness (d_w): (∗) $C^f = 10^{23}$ 1/m^3,$\zeta \approx -2.5$ mV, $d_w = 1$ μm; (+) $C^f = 10^{23}$ 1/m^3, $\zeta \approx -2.5$ mV, $d_w = 0.1$ μm; (△) $C^f = 2 \times 10^{23}$ 1/m^3, $\zeta \approx -5$ mV, $d_w = 1$ μm; (□) $C^f = 2 \times 10^{23}$ 1/m^3, $\zeta \approx -5$ mV, $d_w = 50$ nm; (●) $C^f = 4 \times 10^{23}$ 1/m^3, $\zeta \approx -10$ mV, $d_w = 1$ μm; (◆) $C^f = 4 \times 10^{23}$ 1/m^3, $\zeta \approx -10$ mV, $d_w = 50$ nm. The parameter λ used in the theory to specify the convection in the polymer layer tends to infinity (ref 27, eq 3.18), while the other parameters are specified in Table 1.

The second limit considered corresponds to a particle entirely composed by the wall and is obtained by setting the volume of the internal medium and membrane to very small values ($R_b \ll R_a$). This limit represents an ion-exchange resin (IER) particle and was analytically studied by Grosse and Shilov.[28] Figure 3 shows the numerical spectra obtained for the real part of the dipole coefficient of IER particles (symbols), compared with the corresponding spectra obtained using the theory of Grosse and Shilov for rigid structures (full lines). A very good coincidence between numerical and analytical results is observed in the low-frequency region, for low values of the Donnan potential (The Donnan potential is the value of the equilibrium potential in the electroneutral region of the IER particle.) and high values of the parameter $\kappa_e R_a$. The discrepancies observed at high frequencies were expected because the theory only predicts the counterion polarization (or α dispersion). On the other hand, the discrepancies that appear for smaller values of $\kappa_e R_a$, which are more noticeable for high values of the Donnan

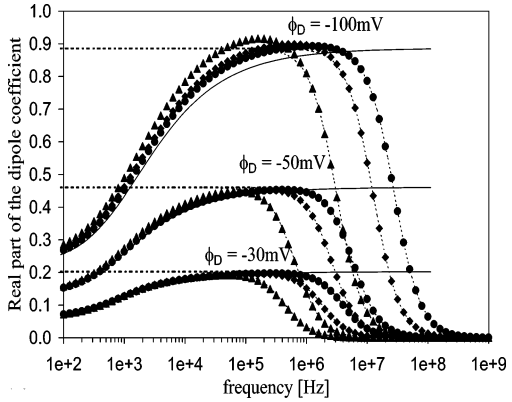

Figure 3. Real part of the dipole coefficient spectra of an IER particle. Comparison between numerical results (symbols) and theoretical predictions according to ref 28 in the low-frequency range (full lines), and a classical Maxwell−Wagner−O'Konsky relaxation in the high-frequency range (dotted lines). The different curves correspond to different values of the Donnan potential (stated in the figure) and of the Debye screening length: $\kappa_e R_a$ = (▲) 50, (◆) 100, (●) 150. The other parameters are specified in Table 1.

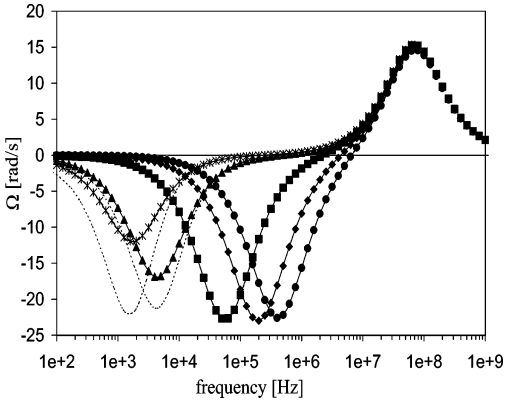

Figure 4. Electrorotation spectra of an uncharged cell. Comparison between numerical results (symbols) and theoretical predictions according to ref 16 (dotted lines) and ref 20 (full lines). The different curves correspond to different values of the Debye screening length: $\kappa_e R_a$ = (∗) 5, (▲) 10, (■) 50, (◆) 100, (●) 150. The other parameters are specified in Table 1.

potential, show that the deviation of the thin double-layer asymptotics (considered in ref 28) from the exact solution increases with the value of the ζ-potential (for a given value of $\kappa_e R_a$). This behavior was noted more than once; see, for example, ref 25. Because of this asymptotic, the theoretical spectra for IER particles are independent of the double-layer thickness. For the high-frequency region, the numerical spectra are compared with the classical Maxwell−Wagner relaxation (dotted lines). The conductivity of the particle, needed for the calculation of this relaxation, was obtained using the equilibrium concentrations of co-ions and counterions near the center of the IER particle, where the potential equals the Donnan potential (ϕ_D):

$$\sigma_p = \frac{e^2}{kT}[(z_e^+)^2 D_w^+ c_{e\infty}^+ \exp(-z_e^+ \tilde{\phi}_D) + (z_e^-)^2 D_w^- c_{e\infty}^- \exp(-z_e^- \tilde{\phi}_D)] \quad (33)$$

This calculation is expected to be valid for thin double layers, and it certainly leads to a very good agreement between analytical and numerical results in all the considered cases.

The last limit considered corresponds to an uncharged cell. This system is particularly interesting because it is possible to obtain an exact analytic solution for the induced dipole coefficient[16] and, consequently, the numerical and analytical results are expected to be identical. However, in the case of the electrorotation spectra, the analytical solution presented in ref 16 uses the additional hypothesis of a thin Debye screening length for the calculation of the electroosmotic contribution. Therefore, the coincidence between the numerical (symbols in Figure 4) and the analytical (dotted lines) spectra is only obtained for high values of the external medium conductivity. To remove the discrepancies observed for thick Debye screening lengths, the electroosmotic contribution was calculated using the second term in eq 31, with a numerical integration.[20] The results obtained (full lines in Figure 4) coincide exactly with the numerical results for all the considered values of the external medium conductivity.

The electrokinetic behavior of cells has been widely studied experimentally and theoretically in the high-frequency range, where the dispersions related to the conductivity and permittivity differences between the media that constitute the system occur.[11,29−36] However, the behavior of cells in the low-frequency range, that is, the frequency range related to the double-layer polarization, has been mainly studied experimentally.[10,12,13,30,35,37,38] As for the few theoretical studies, it was generally assumed that the low-frequency behavior does not depend on the internal composition of the dispersed particle but only on its ζ-potential, so that the theories developed for homogeneous particles can also be used for cells.[12,13,30] To analyze this assumption, cells with different internal compositions were numerically studied, considering different values of the membrane thickness and internal medium conductivity, keeping the charge in the internal medium equal to zero. No dependence with these parameters was observed. On the contrary, when the charge in the internal medium was allowed to change (fixing the value of the potential $\tilde{\phi}_{eq}$) and for low values of both the external medium conductivity and the charge density in the wall, a noticeable change was observed due to the influence of the internal charge on the ζ-potential.

Figures 5−7 show electrorotation spectra numerically obtained for cells as a function of the external medium conductivity (full lines). These figures differ in the value of the fixed charge density in the wall, and since C^f has a constant value for all the curves in every figure, the ζ-potential is different for each curve. The dotted lines represent the theoretical prediction in the high-frequency range, calculated using the results presented in ref 16. The wall conductivity, needed for the analytical calculations, was obtained using eq 33, with the Donnan potential calculated using the electroneutrality condition in the wall. As expected, the numerical and theoretical results are in good agreement for high values of the external medium conductivity, that is, for thin double layers, when the fixed charges are certainly screened inside the wall. For the low-frequency region, no theoretical prediction is presented, since, to our knowledge, there is no electrorotation low-frequency theory valid for particles surrounded by a shell with a volume charge density distribution.

The high-frequency peak observed in Figures 5−7, related to the Maxwell−Wagner−O'Konsky dispersion, does not depend on the external medium conductivity. The characteristic frequency of this dispersion is determined by the highest conductivity in the system that, in the cases considered, is the internal medium conductivity. As this conductivity has a fixed value for the three figures, the peaks do not change either. In the frequency region between 10 kHz and 10 MHz, a second peak can be observed related to the dispersion produced by the presence of the nonconductive membrane. When the membrane is screened by a very conductive wall (produced by a high value

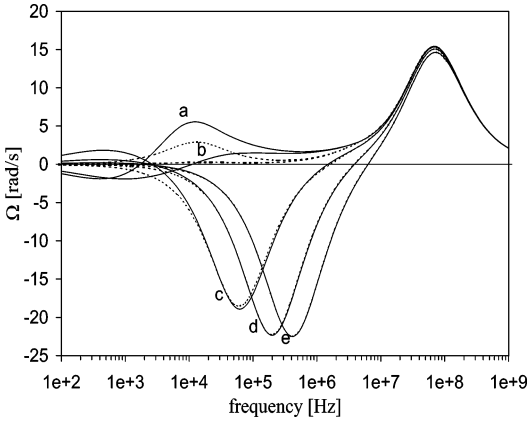

Figure 5. Electrorotation spectra of a cell obtained using numerical (full lines) and high-frequency theoretical calculations[16] (dotted lines) for different values of the Debye screening length: $\kappa_e R_a$ = (a) 5, (b) 10, (c) 50, (d) 100, (e) 150. The fixed charge density is $C^f = 10^{24}$ 1/m^3, so the ζ-potential changes with the medium conductivity: ζ = (a) −163 mV, (b) −128 mV, (c) −48 mV, (d) −21 mV, (e) −11 mV. The other parameters are specified in Table 1.

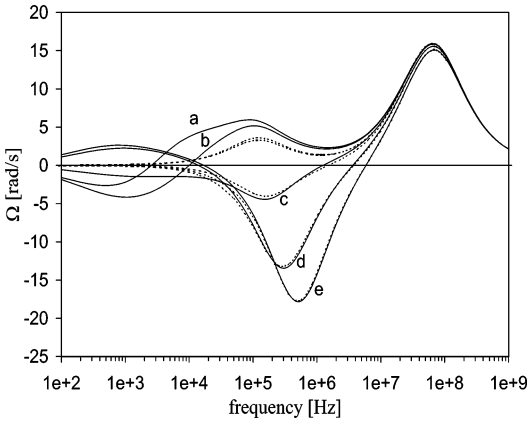

Figure 6. Same as Figure 5, but for $C^f = 10^{25}$ 1/m^3: ζ = (a) −223 mV, (b) −188 mV, (c) −105 mV, (d) −70 mV, (e) −51 mV.

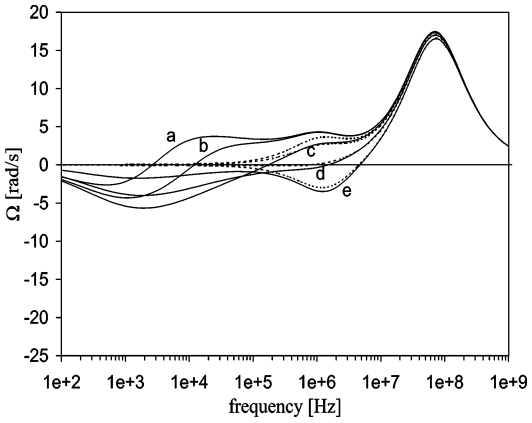

Figure 7. Same as Figure 5, but for $C^f = 10^{26}$ 1/m^3: ζ = (a) −284 mV, (b) −248 mV, (c) −164 mV, (d) −129 mV, (e) −108 mV.

of the fixed charge density), the dispersion process is less important, and the peak amplitude is lowered. This can be observed comparing Figures 5−7, where, for example, the negative peaks in curves e reduce their amplitude when C^f increases. In the low-frequency range, the spectra present a third rotation peak related to the double-layer polarization. This peak is positive for low values of the ζ-potential, when the electroosmotic term dominates the rotation, while it is negative for higher values of the ζ-potential, when the real part of the dipole

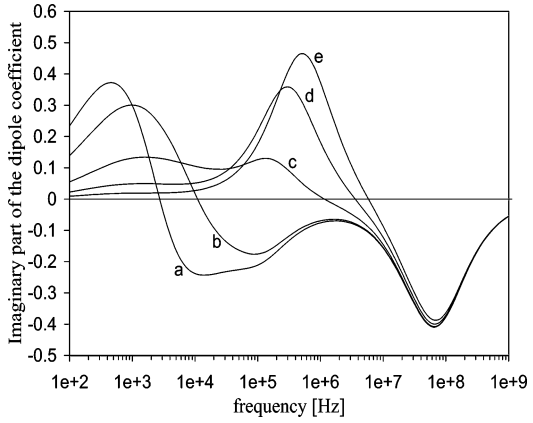

Figure 8. Imaginary part of the dipole coefficient spectra of a cell calculated numerically, for the same systems as in Figure 6.

coefficient changes significantly through the dispersion, and the classical term dominates the rotation. As the fixed charge density has a constant value in each of Figures 5−7, the ζ-potential changes with the external medium conductivity, leading to either positive or negative rotation peaks depending on the ζ-potential value. This last behavior can be clarified with the help of Figure 8, where the imaginary parts of the dipole coefficient spectra corresponding to the same systems considered in Figure 6 are represented. As can be seen, the curves appearing in Figures 6 and 8 are similar for high frequencies (except for the sign), showing that the electrorotation velocity is approximately proportional to the imaginary part of the dipole coefficient (classical result, first term in eq 31). However, the low-frequency peaks appearing in Figure 8 are all positive while they change sign in Figure 6. This shows explicitly the importance of the electroosmotic term (second term in eq 31) in the low-frequency region.

Finally, experimental electrorotation data of yeast cells obtained by Hölzel[11] are presented in Figure 9 and compared with numerical results obtained using the parameters in Table 2. In his paper, Hölzel simulates the experimental results with a four shell model, obtaining a very good agreement for the medium- and high-frequency ranges, but cannot predict any low-frequency rotation. On the other hand, our numerical results lead to a very good agreement for the medium- and low-frequency ranges and a fair agreement for high frequencies. This last discrepancy is expected to be removed, as demonstrated by Hölzel, including an inner wall and a periplasmic space. As a final remark, it is important to note that the same cell

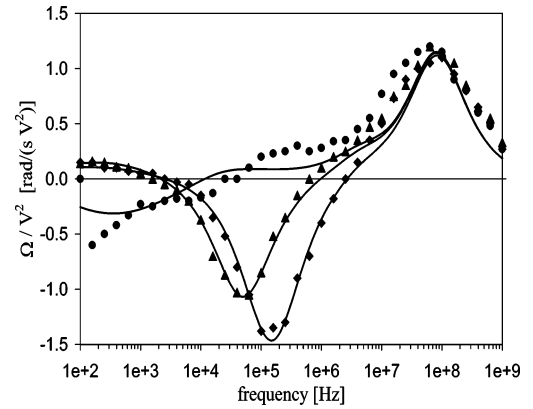

Figure 9. Experimental electrorotation spectra of yeast cells obtained by Hölzel[11] at different medium conductivities (symbols), compared with numerical results (lines). σ_e = (●) 0.7 μS/cm, (▲) 20 μS/cm, (◆) 90 μS/cm. The other parameters are specified in Table 2.

TABLE 1: Parameter Values Used in Figures 2−8

$R_a = 1.5\ \mu$m	$z_e^{\pm} = z_i^{\pm} = \pm 1$	$\rho^m = 10^3$ kg/m^3
$R_b - R_c = 5$ nm	$D_e^{\pm} = D_w^{\pm} = D_i^{\pm} =$	$\rho^p = 1.2 \times 10^3$ kg/m^3
$\epsilon_e = 78.36$	2×10^{-9} m^2/s	$\eta = 8.904 \times 10^{-4}$ Pa s
$\epsilon_m = 4$	$z^f = -1$	$E = 10000$ V/m
	$\phi_{eq} = 0$ V	$T = 298.4$ K

	Figure 2	Figure 3	Figures 4−8
$R_a - R_b =$		1.48 μm	50 nm
$\epsilon_i =$	4	4	70
$\sigma_i =$	0 S/m	0 S/m	0.8 S/m
$\kappa_e R_a =$	100		

TABLE 2: Parameter Values Used in Figure 9

$R_a = 3.2\ \mu$m	$\sigma_i = 0.9$ S/m	$\phi_{eq} = 0$ V
$R_a - R_b = 185$ nm	$z_e^{\pm} = z_i^{\pm} = \pm 1$	$\rho^m = 10^3$ kg/m^3
$R_b - R_c = 3.5$ nm	$D_e^{\pm} = D_w^{\pm} = D_i^{\pm} =$	$\rho^p = 1.2 \times 10^3$ kg/m^3
$\epsilon_e = 78$	2×10^{-9} m^2/s	$\eta = 4.9 \times 10^{-4}$ Pa s
$\epsilon_m = 3$	$C^f = 1.7 \times 10^{24}$ 1/m^3	$T = 298.4$ K
$\epsilon_i = 51$	$z^f = -1$	electrode sep = 520 μm

parameters were used to obtain the three numerical spectra in Figure 9 (only the external medium conductivity was changed), showing that the fixed charge in the cell appears to be independent of the external medium conductivity, at least in the considered cases.

Acknowledgment. This work was partially supported by Grant 26/E220 of the Consejo de Investigaciones de la Universidad Nacional de Tucumán and by FOMEC and FACEyT fellowships to V.Z.

Appendix

The boundary condition for the vorticity is obtained considering the balance of forces on the particle surface,[3]

$$\vec{F}_{mech}(R_a,t) + \vec{F}_{elec}(R_a,t) = \frac{4\pi}{3} R_a^3 \rho^p \frac{\partial \vec{v}(R_a,t)}{\partial t} \qquad (34)$$

where $\vec{F}_{mech}$ and $\vec{F}_{elec}$ are the mechanic and electric forces acting on the particle, respectively, and ρ^p is the average mass density of the particle (the symbols + after R_a in the arguments of the functions are omitted in order to simplify the notation).

Mechanic Force. This force (that includes the viscous and pressure forces) is obtained by integrating the stress tensor on the particle surface,

$$\vec{F}_{mech}(r,t) = \int_S (\sigma_{rr}\hat{e}_r + \sigma_{\theta r}\hat{e}_\theta + \sigma_{\psi r}\hat{e}_\psi)\, ds$$

where $\hat{e}_r$, $\hat{e}_\theta$, and $\hat{e}_\psi$ are the unit vectors corresponding to a spherical coordinate system centered on the particle and with the polar axis parallel to the applied field. σ_{rr}, $\sigma_{\theta r}$, and $\sigma_{\psi r}$ are the stress tensor components,

$$\sigma_{rr} = 2\eta \frac{\partial v_r(r,t)}{\partial r} \cos\theta - p(r,t)\cos\theta$$

$$\sigma_{\theta r} = -\eta\left[r\frac{\partial}{\partial r}\left(\frac{v_\theta(r,t)}{r}\right) + \frac{v_r(r,t)}{r}\right]\sin\theta$$

and $\sigma_{\psi r} = 0$ due to symmetry. Substituting these expressions in the integral and taking into account that only the component parallel to the polar axis can contribute to the force leads to

$$\vec{F}_{mech}(r,t) = \int_S (\sigma_{rr}\cos\theta - \sigma_{\theta r}\sin\theta)\, ds\, \hat{k} = \left\{\frac{8\pi}{3}\eta r^2 \frac{\partial v_r(r,t)}{\partial r} - \frac{4\pi}{3} r^2 p(r,t) + \frac{8\pi}{3}\eta r^2\left[r\frac{\partial}{\partial r}\left(\frac{v_\theta(r,t)}{r}\right) + \frac{v_r(r,t)}{r}\right]\right\}\hat{k}$$

where $\hat{k}$ is a unit vector in the direction of the polar axis, or

$$\vec{F}_{mech}(R_a,t) = \frac{4\pi}{3}R_a^2\left[2\eta\left[\frac{\partial v_r(r,t)}{\partial r}\Big|_{R_a} + R_a\frac{\partial}{\partial r}\left(\frac{v_\theta(r,t)}{r}\right)\Big|_{R_a} + \frac{v_r(R_a,t)}{R_a}\right] - p(R_a,t)\right]\hat{k}$$

$$= \frac{4\pi}{3}R_a^2\left[2\eta\frac{\partial v_\theta(r,t)}{\partial r}\Big|_{R_a} - p(R_a,t)\right]\hat{k}$$

$$= -\frac{4\pi}{3}R_a^2[2\eta b(R_a,t) + p(R_a,t)]\hat{k} \qquad (35)$$

where the derivative of the velocity was replaced by the vorticity according to its definition, and the boundary conditions of null velocity ($v_r(R_a,t) = 0$, $v_\theta(R_a,t) = 0$) and null variation of the normal component of the velocity on the surface ($\partial v_r(r,t)/\partial r|_{R_a} = 0$) were considered. These last conditions are valid on an inertial reference frame that instantly moves with the same velocity as the particle. From this reference frame, the liquid velocity next to the surface is null but its acceleration is not null. Moreover, the velocity very far from the particle is not null either, but its value is minus the velocity of the particle with respect to a laboratory reference frame. As a consequence, the acceleration of the liquid next to the particle (or acceleration of the particle) can be calculated as minus the temporal derivative of the liquid velocity very far from the particle. Even though the liquid is not accelerated very far from the particle, the temporal dependence of the variables is solved by changing the reference frame as to keep null the velocity of the particle. Consequently, the velocity at infinity changes with time in the same way as the velocity of the particle changes with respect to the laboratory reference frame (except for the sign).

To obtain the pressure, the tangential component of the Navier−Stokes equation (eq 5) is considered,

$$\eta\nabla^2\vec{v}(\vec{r},t)|_\theta - \nabla_\theta p(\vec{r},t) = \rho(\vec{r},t)\,\nabla_\theta\phi(\vec{r},t) + \rho^m\frac{\partial v(\vec{r},t)}{\partial t}\Big|_\theta \qquad R_a < r < \infty \quad (36)$$

where $\rho(\vec{r},t) = e(z_e^+C^+(\vec{r},t) + z_e^-C^-(\vec{r},t))$ is the charge density and the last term in the complete Navier−Stokes equation is neglected because it is of second order on the field. Writing the first addend in terms of the vorticity and expanding the derivative operators leads to

$$-\eta\left[\frac{1}{r\sin\theta}\frac{\partial b_r(\vec{r},t)}{\partial\psi} - \frac{1}{r}\frac{\partial}{\partial r}(rb_\psi(\vec{r},t))\right] - \frac{1}{r}\frac{\partial p(\vec{r},t)}{\partial\theta} = \rho_0(r)\frac{1}{r}\frac{\partial\delta\phi(\vec{r},t)}{\partial\theta} + \rho^m\frac{\partial v(\vec{r},t)}{\partial t}\Big|_\theta \quad R_a < r < \infty$$

where the ion number concentrations and electric potential were written in terms of their equilibrium and field induced variations components, and the terms in second order of the field were

neglected. Considering the angular dependence of the variables, the pressure on the surface results

$$p(R_a,t) = -\rho_0(R_a)\,\delta\phi(R_a,t) - \eta\left(R_a \left.\frac{\partial b(r,t)}{\partial r}\right|_{R_a} + b(R_a,t)\right) - \rho^m R_a \frac{\partial v_\theta(R_a,t)}{\partial t}$$

Replacing this equation in eq 35 leads to the following expression for the mechanic force,

$$\vec{F}_{mech}(R_a,t) = \frac{4\pi}{3}R_a^2\left[\rho_0(R_a)\,\delta\phi(R_a,t) + \rho^m R_a \frac{\partial v_\theta(R_a,t)}{\partial t} + \eta\left(R_a \left.\frac{\partial b(r,t)}{\partial r}\right|_{R_a} - b(R_a,t)\right)\right]\hat{k} \quad (37)$$

Electric Force. The electric force acting on the particle ($\vec{F}_{elec}(R_a,t)$) is obtained by calculating the electric force acting on the liquid: since the electric force on an electroneutral system must be null, the electric force on the particle is minus the electric force on the liquid,

$$\vec{F}_{elec}(R_a,t) = \int_0^{2\pi}\int_0^{\pi}\int_{R_a}^{\infty}\rho(\vec{r},t)\,\nabla\phi(\vec{r},t)\,r^2\sin\theta\,dr\,d\theta\,d\psi$$

In the same way as for the mechanic force, only the component parallel to the polar axis can contribute to the force, leading to

$$\vec{F}_{elec}(R_a,t) = \frac{4\pi}{3}\int_{R_a}^{\infty}\left[\rho_0(r)\frac{\partial\delta\phi(r,t)}{\partial r}r^2 + 2\rho_0(r)\,\delta\phi(r,t)\,r + \delta\rho(r,t)\frac{d\phi_0(r)}{dr}r^2\right]dr\,\hat{k}$$

$$= \frac{4\pi}{3}\int_{R_a}^{\infty}\frac{\partial}{\partial r}(\rho_0(r)\,\delta\phi(r,t)\,r^2)\,dr\,\hat{k} + \frac{4\pi}{3}\int_{R_a}^{\infty}\left[\delta\rho(r,t)\frac{d\phi_0(r)}{dr} - \delta\phi(r,t)\frac{d\rho_0(r)}{dr}\right]r^2\,dr\,\hat{k}$$

$$= -\frac{4\pi}{3}R_a^2\rho_0(R_a)\,\delta\phi(R_a,t)\,\hat{k} + \frac{4\pi}{3}e\int_{R_a}^{\infty}[z_e^+C_0^+(r)\,\delta\tilde{\mu}^+(r,t) + z_e^-C_0^-(r)\,\delta\tilde{\mu}^-(r,t)]\times\frac{d\phi_0(r)}{dr}r^2\,dr\,\hat{k} \quad (38)$$

where the charge density and electric potential were written in terms of their equilibrium and field induced variation components.

Finally, replacing the mechanic and electric forces (eqs 37 and 38) in eq 34 leads to

$$\frac{4\pi}{3}R_a^3\rho^m\frac{\partial v_\theta(R_a,t)}{\partial t}\hat{k} + \frac{4\pi}{3}R_a^2\,\eta\left(R_a\left.\frac{\partial b(r,t)}{\partial r}\right|_{R_a} - b(R_a,t)\right)\hat{k} + \frac{4\pi}{3}e\int_{R_a}^{\infty}[z_e^+C_0^+(r)\,\delta\tilde{\mu}^+(r,t) + z_e^-C_0^-(r)\,\delta\tilde{\mu}^-(r,t)]\times\frac{d\phi_0(r)}{dr}r^2\,dr\,\hat{k} = \frac{4\pi}{3}R_a^3\rho^p\frac{\partial}{\partial t}(v_r(R_a,t)\cos^2\theta + v_\theta(R_a,t)\sin^2\theta)\hat{k}$$

where the velocity in the second member was projected over the polar axis. As previously said, the acceleration terms are calculated using the velocity at infinity, where the radial and polar components of the velocity have the same value. Thus, the boundary condition finally results in

$$b(R_a,t) - R_a\left.\frac{\partial b(r,t)}{\partial r}\right|_{R_a} = \frac{R_a(\rho^m-\rho^p)}{\eta}\frac{\partial v_r(R_a,t)}{\partial t} + \frac{kT}{R_a^2\eta}\int_{R_a}^{\infty}[z_e^+C_0^+(r)\,\delta\tilde{\mu}^+(r,t) + z_e^-C_0^-(r)\,\delta\tilde{\mu}^-(r,t)]\frac{d\tilde{\phi}_0(r)}{dr}r^2\,dr$$

Supporting Information Available: Spatial variables ξ used in each medium for the numerical solution of the problem. Schematic representation of the whole network used to solve the equation system. Values of the resistances (R), capacitors (C), current sources (I), voltage controlled current sources (G), and voltage controlled voltage sources (E) used in the circuit. This material is available free of charge via the Internet at http://pubs.acs.org.

References and Notes

(1) O'Brien, R. W.; White, L. R. *J. Chem. Soc., Faraday Trans.* **1978**, *74*, 1607−1626.

(2) DeLacey, E. H.; White, L. R. *J. Chem. Soc., Faraday Trans.* **1981**, *77*, 2007−2039.

(3) Mangelsdorf, C. S.; White, L. R. *J. Chem. Soc., Faraday Trans.* **1992**, *88*, 3567−3581.

(4) Mangelsdorf, C. S.; White, L. R. *J. Chem. Soc., Faraday Trans.* **1997**, *93*, 3145−3154.

(5) López-Garcıa, J. J.; Horno, J.; González-Caballero, F.; Grosse, C.; Delgado, A. V. *J. Colloid Interface Sci.* **2000**, *228*, 95−104.

(6) Saville, D. *J. Colloid Interface Sci.* **2000**, *222*, 137−145.

(7) López-Garcıa, J. J.; Grosse, C.; Horno, J. *J. Colloid Interface Sci.* **2002**, *254*, 287−295.

(8) Arnold, W. M.; Geier, B. M.; Wendt, B.; Zimmermann, U. *Biochim. Biophys. Acta* **1986**, *889*, 35−48.

(9) Hu, X.; Arnold, W. M.; Zimmermann, U. *Biochim. Biophys. Acta* **1990**, *1021*, 191−200.

(10) Zhou, X.-F.; Markx, G. H.; Pethig, R.; Eastwood, I. M. *Biochim. Biophys. Acta* **1995**, *1245*, 85−93.

(11) Hölzel, R. *Biophys. J.* **1997**, *73*, 1103−1109.

(12) Neu, B.; Georgieva, R.; Bäumler, H.; Shilov, V. N.; Knippel, E.; Donath, E. *Colloids Surf., A* **1998**, *140*, 325−332.

(13) Georgieva, R.; Neu, B.; Shilov, V. N.; Knippel, E.; Budde, A.; Latza, R.; Donath, E.; Kiesewetter, H.; Bäumler, H. *Biophys. J.* **1998**, *74*, 2114−2120.

(14) Kakutani, T.; Shibatani, S.; Sugai, M. *Bioelectrochem. Bioenerg.* **1993**, *31*, 131−145.

(15) Zimmerman, V.; Grosse, C.; Shilov, V. N. *Colloids Surf., A* **1999**, *159*, 299−309.

(16) Zimmerman, V.; Grosse, C. *Colloids Surf., A* **2002**, *197*, 69−77.

(17) Horno, J.; González-Fernández, C.; Hayas, A.; González-Caballero, F. *Biophys. J.* **1989**, *55*, 527−535.

(18) Shilov, V. N.; Delgado, A. V.; González-Caballero, F.; Horno, J.; López-Garcıa, J. J.; Grosse, C. *J. Colloid Interface Sci.* **2000**, *232*, 141−148.

(19) López-Garcıa, J. J.; Horno, J.; Delgado, A. V.; González-Caballero, F. *J. Phys. Chem. B* **1999**, *103*, 11297−11307.

(20) Zimmerman, V.; Shilov, V. N.; López-Garcıa, J. J.; Grosse, C. *J. Phys. Chem. B* **2002**, *106*, 13384−13392.

(21) Einolf, C. W., Jr.; Carstensen, E. L. *J. Phys. Chem.* **1971**, *75*, 1091−1099.

(22) Born, M. *Z. Physik* **1920**, *1*, 45−48.

(23) Shilov, V. N. *Colloids Surf., A* **1998**, *142*, 375−379.

(24) Grosse, C.; Shilov, V. N. *J. Phys. Chem.* **1996**, *100*, 1771−1778.

(25) Grosse, C.; Arroyo, F.; Shilov, V. N.; Delgado, A. V. *J. Colloid Interface Sci.* **2001**, *242*, 75−81.

(26) Arnold, W. M.; Schwan, H. P.; Zimmermann, U. *J. Phys. Chem.* **1987**, *91*, 5093−5098.

(27) Ohshima, H. *J. Colloid Interface Sci.* **2001**, *233*, 142−152.

(28) Grosse, C.; Shilov, V. N. *J. Colloid Interface Sci.* **1996**, *178*, 18−28.

(29) Carstensen, E. L. *Biophys. J.* **1967**, *7*, 493−503.

(30) Fuhr, G.; Kuzmin, P. I. *Biophys. J.* **1986**, *50*, 789−795.

(31) Fuhr, G.; Hagedorn, R. Cell electrorotation. In *Electrical Manipulation of cells*; Lynch, P., Davey, M., Eds.; Chapman and Hall: New York, 1996.
(32) Schwan, H. P. *Ferroelectrics* **1988**, *86*, 205−223.
(33) Arnold, W. M.; Zimmermann, U. *Z. Naturforsch.* **1982**, *37*, 908−915.
(34) Arnold, W. M.; Zimmermann, U. *J. Electrostat.* **1988**, *21*, 151−191.
(35) Foster, K. R.; Schwan, H. P. *CRC Crit. Rev. Biomed. Eng.* **1989**, *17*, 25−104.
(36) Asami, K.; Yonezawa, T. *Biophys. J.* **1996**, *71*, 2192−2200.
(37) Einolf, C. W., Jr.; Carstensen, E. L. *Biophys. J.* **1969**, *9*, 634−643.
(38) Foster, K. R.; Sauer, F. A.; Schwan, H. P. *Biophys. J.* **1992**, *63*, 180−190.